npj | heritage science

Article

https://doi.org/10.1038/s40494-025-02060-8

Computer-based method to digitally reconstruct axially symmetric fragmented heritage: the case of a medieval bell

Check for updates

Luca Di Angelo[1,2], Paolo Di Stefano[1,2], Rocco Furferi[3] ✉, Lapo Governi[3] & Emanuele Guardiani[1,2]

The shape and tuning of bells provide archaeologists with valuable insights into their historical origins and casting methods. Unfortunately, the availability of fully preserved medieval and Renaissance bells is limited worldwide due to the remelting of many specimens following fractures, wear, or traumatic events such as earthquakes. The original geometry is therefore reconstructed by archaeologists by examining uncovered external mould during excavations. However, determining the symmetry axis and interpreting the profiles of small fragments is not trivial, and fragments are not always easily reassembled along their fracture surfaces. To solve this issue, this paper presents a computer-based method that enables the automated virtual reconstruction of ancient bells from their external mould fragments. The approach performs geometric and differential analysis of discrete models obtained from 3D scans of the fragments, facilitating the retrieval of a consistent 3D shape, thereby aiding in the preservation and understanding of historical relics.

The art of bell formation did not reach its pinnacle in Europe until the 17th century, even though bronze bells with exceptional melodic qualities "were cast in China around 3000 years ago"[1,2]. This period marked a significant development with the Hemony brothers, who successfully designed and cast the first precisely tuned carillon. They discovered the ideal shaping of the bell profile, ensuring that the ratios of their vibrational frequencies adhered to musical relationships. This tuning resulted in bells with strong tonal characteristics and improved musical pitch, enabling melodies and chords to be played from a set of bells. The first experiments with copper-tin alloys for bell casting in Europe are believed to have taken place in the fourth century[3]. During this time, bells were primarily used for practical purposes, such as regulating daily activities and commemorating rites, rather than for polyphonic music[3]. Consequently, musicality and tuning quality were of lesser importance. By the early 12th century, bell design underwent a significant transformation, moving from conical shapes to the more curved profiles we recognize today. This gradual evolution enhanced the sound characteristics of the bells, resulting in a more pleasant tone[2]. Based on previous considerations, the morphology and tuning of the bells offer valuable insights into their place of origin, reflecting the casting and tuning techniques employed during their creation. Since the 1980s, advances in technology and computational power have significantly improved the physical modelling and simulation of the dynamic behaviour of musical instruments[4,5]. A review of the existing literature reveals various approaches to analysing several aspects of bell acoustics. These include analysis of bell vibration modes[6–8], the impact of bell geometry on sound[9], the study of materials used in bell casting[10], the dynamic responses of bells to external excitation[11–14] and "the development of physics-based sound synthesis techniques"[2]. Studies dealing with the analysis of bell vibrations are also provided by scientific literature[15–17]. Unfortunately, accurate 3D geometrical data from bells acquired using structured light scanning are barely explored in the literature and only in refs. 16,17 some valuable hints are provided. As a result, due to the lack of automated or computer-based methods, archaeologists reconstruct bells using manual methods.

Archaeological excavations sometimes reveal only remnants of these bells, melting pots that are often broken into fragments[18]. Archaeologists study these findings to learn more about bell forms and casting methods. The axis and generator profile are estimated by hand from the fragments of the casting mantle and then depicted in drawings. The final shape of the bell is constructed by merging these drawings. Unfortunately, fragments rarely include features that could help determine their orientation in the three-dimensional space, such as axially symmetric decorations[19]. In addition, archaeologists work with small fragments that are not trivial to put together along their fracture surfaces, due to the damage incurred while the bells were extracted from the earth. Accordingly, to the best of the authors' knowledge, developing a computer-based technique for assembling the bell's geometry from the external mould fragments is a groundbreaking innovation for the

[1]Department of Industrial and Information Engineering and Economics, University of L'Aquila, Piazzale Pontieri, 1, Monteluco di Roio, L'Aquila, Italy. [2]Heritechne, University of L'Aquila, Piazzale Pontieri, 1, Monteluco di Roio, L'Aquila, Italy. [3]Department of Industrial Engineering, University of Florence, Via di S. Marta, 3, Firenze, Italy. ✉e-mail: rocco.furferi@unifi.it

Cultural Heritage field. In fact, besides the lack of methods developed by the scientific community on bell reconstruction, even the methods provided by scientific literature dealing with reconstructing other axially symmetric objects from fragments are not directly employable.

As noted in ref. 20, both local and global techniques available "rely on reassembling the original complete geometry by connecting the fragments in correspondence of their fracture surfaces". Furthermore, "due to the damage to the external mould caused by the removal of the bell, as well as considerable wear, encrustations, and other common damage to archaeological shards, the item cannot be reassembled simply by reassembling the pieces at their fractured edges"[20].

To overcome these limitations, the present work aims to provide a computer-based technique to restore the shape of the bell using external mould fragments. The method uses discrete models of fragments, which are obtained via a 3D scanner, and a specifically developed geometric-differential analysis. This technique generates a 3D shape of the bell that is compliant with the actual shapes of bells from the same area and period when applied to pieces from a medieval bell furnace. For the digital reconstruction of items of axially symmetric cultural heritage that cannot be put back together along fractured surfaces, this novel method holds promise. Thus, it could be an invaluable instrument for understanding and preserving historical items in the context of cultural heritage conservation.

Methods

The approach described in the present article originates from the analysis of 35 fragments (see Fig. 1) of a bell furnace located in Rocca di Cambio (Italy) that may date to the second half of the 13th century[18]. These fragments are not from the bell itself but from the external mould (casting mantle) used to shape the bell during the lost-wax casting process. This mould, found in a 13th-century bell furnace discovered in Rocca di Cambio, Italy[18,21], was made of clay that was formed into two different layers, according to the examination of these well-preserved pieces. The rough and coarse clay exterior layer that was exposed to fire has calcareous inclusions and evident plant material traces, such as straw or manure, which provide enough porosity.

Archaeologists established the following details from the macroscopic examination of casting mantle fragments:

- the bell had to have been 3.2 cm thick, with a decoration at shoulder level that was characterized by a convex band surrounded by two cords in relief;
- the remaining portion of the body, which was smooth and devoid of macroscopic impurities or imperfections, "was occupied by at least four concentric lines that were 1.6 cm apart and situated in the hollow of the bell, between the lip and the inscription"[22].

The method proposed in this work is structured in four key steps (see Fig. 2):

1. Fragments digital twin generation
2. Features segmentation and recognition
3. 2D profile reconstruction
4. 3D virtual reconstruction

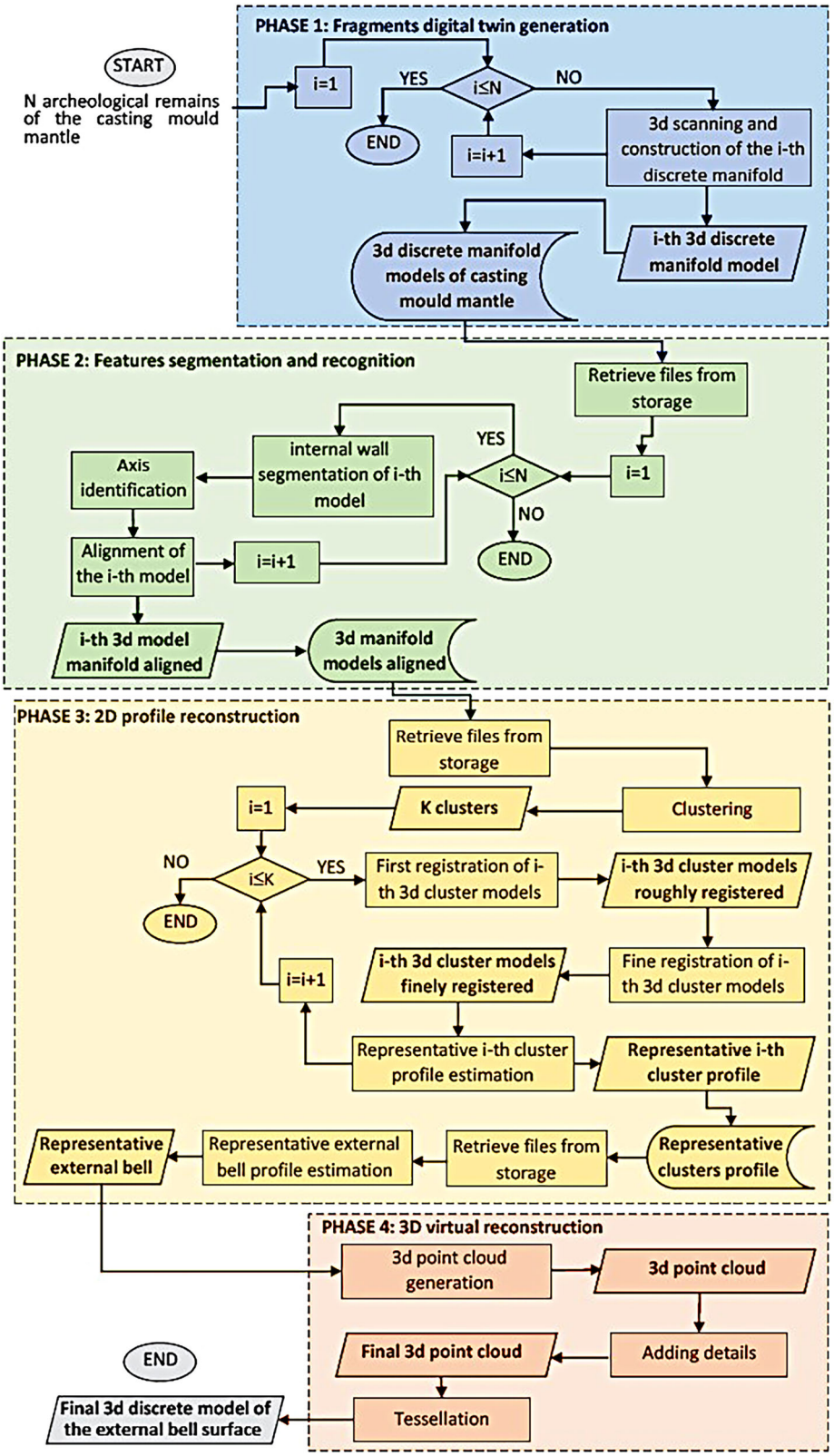
Fragments digital twin generation

The first step consists in digitizing fragments belonging to the external mould used to shape the bell during the lost-wax casting process. Since even



Fig. 1 | The 35 fragments related to the bell furnace here considered.

Fig. 2 | Flow-chart of the proposed method.



a fragment cannot always be acquired in a single scan, mainly due to its dimensions and the limitations of scanning technology, multiple scans are often required, each taken from a specific orientation of the object relative to the scanning device.

Consequently, the acquired point clouds must be aligned in the same reference system through a registration process[23]. Once point clouds are appropriately registered, outliers are manually removed (e.g., using radius-based or clustering-based outlier removal method[24], clouds are resampled and smoothed, and mesh refinement and remeshing is carried out using Laplacian smoothing filters[25].

The results of this process, which is the only non-automated step in the proposed procedure, can "vary based on the operator's subjectivity, expertise, skills, and professional experience" according to scientific literature[17].

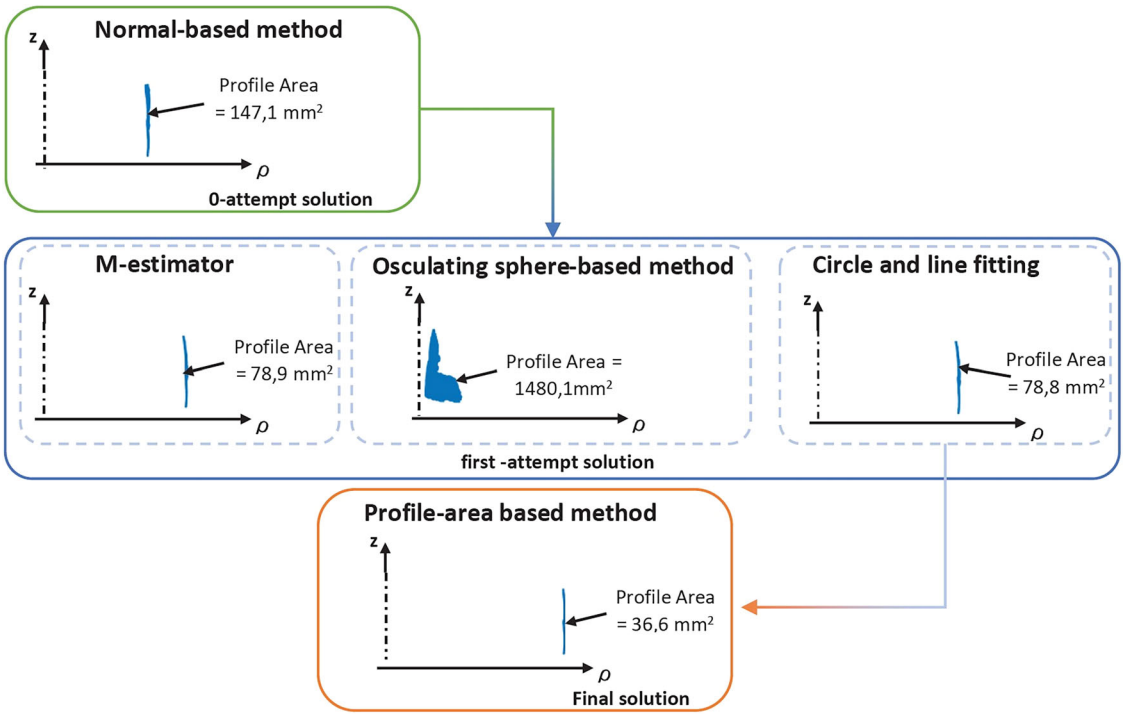


Fig. 3 | The symmetry axis detection methodology.

Features segmentation and recognition

Smooth regions need to be identified to segment the smoothest inner surface of each fragment. This is accomplished by locating large areas of the fragment's surface that have the so-called *sharpness indicator* (SHI)[26] value below a given threshold. The SHI measures the C^1 continuities of the ~~h-ring~~ n-ring neighbourhood of a triangular mesh i.e., the set of vertices that are "n steps" away from a given vertex. By using a sphere to approximate the segmentation points and checking the concavity by its normal vertices, the interior wall of the casting mould mantle can be recognized.

The smooth axisymmetric inner part needs to be processed to determine its symmetry axis. Generally, evaluating the axis of symmetry is a complex task that influences subsequent analyses. These challenges arise because the only information from a discrete model is limited to the coordinates of points and the normal of triangles. As highlighted in the literature[27], these difficulties are overstated when analysing fragments in Cultural Heritage. Based on these considerations, this paper employs an iterative method to obtain the best axis of symmetry that starts with an initial solution and undergoes further refinement 3). The initial solution represents the best outcome achieved using the following methods, which are considered state-of-the-art as of now:

- normal based,
- M-estimator,
- osculating sphere-based,
- circle and line fitting method.

It is important to note that M-estimators, osculating sphere-based, and circle and line fitting methods are iterative and require an initial solution. The proposed methodology initialises these methods using the normal-based solution (see Fig. 3). The aforementioned methods rely on the indirect properties of axisymmetric surfaces.

Hence, as reported in[20], none of these approaches yields accurate results for fragments with incomplete circular spans, particularly when low point cloud density is affected by micro and macro irregularities.

For these reasons, the implemented procedure con- siders the typical manufacturing method used to create the casting mantle, whose fragments must be analysed, was constructed: a profiling compass was rotated around a central pivot to shape and smooth the curved surface. The initial solution minimizes the profile area obtained through the three methods (the first attempt solution box as illustrated in the figure). This profile area is calculated by projecting the 3D coordinates of points identified as axially symmetric onto the 2D cylindrical coordinates (ρ, **z**), with the evaluated axis coinciding with the **z** *axis* of the global reference system. If the surface were a perfect surface of revolution and the axis were accurate, the projected profile would converge to a strict geometrical curve, resulting in a profile area of zero. However, surface deformations on a macroscopic or microscopic scale and inaccuracies in the axis create a strip of projected axially symmetric points. Therefore, starting from the initial solution, the final solution is achieved by iteratively minimizing the profile area using the Levenberg-Marquardt algorithm[28].

All bell fragments are processed using the aforementioned iterative process so that each part is eventually aligned and its fragment axis (α) coincides with the z-axis.

2D profile reconstruction

The 2D profile reconstruction phase begins with the clustering of 3D sherds (see Fig. 2). This process involves grouping fragments with similar radius values. After clustering, the fragments must be registered to allocate the final two degrees of freedom, i.e., the z-coordinate (parallel to the axis) and the θ-coordinate (which indicates the rotation angle around the axis). This is accomplished by performing coarse and refined registration so that the fragments with the greatest extension along the z-axis of each cluster are fixed in place. The remaining fragments are eventually arranged to maximize the overlapping areas of their distances from the axis.

In detail, coarse registration is achieved by determining Δz and $\Delta\theta$ values, minimizing the distance between each fragment analysed and previously registered ones. The configuration obtained from the coarse registration is refined by minimizing the objective function provided by the following Equation:

$$\left[\Delta z^{opt}\,\Delta\theta^{opt}\right] = \arg\min_{\Delta z,\Delta\theta}\left|\left|\frac{1}{f_1 f_2}\right|\right| \quad (1)$$

Table 1 | Input parameters required by the proposed method

Proposed method phase	Parameter	Description	Value
Features segmentation and recognition	n_h	Neighbourhood order	3
Features segmentation and recognition	τSHI	Smoothness indicator threshold value	0.05
2D profile reconstruction	*tol* 1	Distance threshold value (see Eq. 2)	1.0 mm
2D profile reconstruction	*tol* 2	Distance threshold value (see Eq. 3)	1.0 mm
2D profile reconstruction	N_{iter}	Number of iterations of the minimization process	10

Where:

- N is the number of points $\wp_{moving}$ (i.e., the points which change coordinates during the registration process)
- D is a $M \times N$ matrix, defined as follows:

$$D_{M\times N} = \begin{cases} d_{i,j} = distance(\mathcal{p}_i \in \mathcal{p}_{fixed}, j \in \mathcal{p}_{aligned}) & if\ distance < tol_{f1} \\ d_{i,j} = NULL & otherwise \end{cases} \quad (2)$$

- $d_{i,j}$ is a non-null element representing the Euclidean distance between the ith point of $\mathcal{P}_{fixed}$ and the j-th point of $\mathcal{P}_{moving}$; this is defined only when it is lower than the threshold value *tol*;
- $f_2 = \frac{\sum_{i,j}^{M,N} v_{i,j}}{|D|}$ is a term that refines the angular mismatch between the two point clouds; in this formulation, $v_{i,j}$ are the elements of a $M \times N$ matrix $V_{M\times N}$ defined as follows:

$$V_{M\times N} = \begin{cases} v_{i,j} = \hat{n}(\boldsymbol{P}_i) \cdot \hat{n}(\boldsymbol{Q}_i)\ \textbf{if}\ d_{i,j} < tol_{f2} \\ v_{i,j} = NULL\ otherwise \end{cases} \quad (3)$$

being $\hat{n}(\boldsymbol{P}_i)$ the exterior normal estimated at the point $\boldsymbol{P}_i$.

This minimization process realigns all point clouds by "registering pairs between one randomly selected cloud (designated as fixed) and all other clouds". This registration is repeated N_{iter} times across N fragments. Fragments belonging to the same cluster and finely registered are then processed to determine a new symmetry axis.

Once established, these fragments are realigned so that the new axis aligns with the z-axis. Finally, the series of circles' radii, which indicate the crossings of planes perpendicular to the z-axis, is measured using finely aligned fragments to construct the cluster profile. More details of this procedure are presented in ref. 29.

An algorithm has been appropriately devised to fill in the missing areas of the original bell profile, allowing for the reconstruction of a representative external bell profile where no fragments were found. This algorithm calculates the optimal translation along the z-axis (in the z-ρ plane) of one profile in relation to another, ensuring that the smoothest possible curve is obtained by extrapolating between the two profiles. Specifically, the proposed algorithm aligns two profile datasets at a time (designated as *profile_f* and *profile_m*), which represent fragments of a larger 2D profile, by minimizing the following:

$$E = \frac{1}{N}\sum_{i=1}^{N}\left[z_f(\rho_i) - z_m(\rho_i) * (1 - n_f(\rho_i) * n_i(\rho_i)\right]^2 \quad (4)$$

Where:

- N is the size of $\rho_{common} = [\max(\min(\rho_f), \min(\rho_m)), \min(\max(\rho_f), \max(\rho_m))]$ that is the ρ interval in which the profile is to be reconstructed;
- $z_f(\rho_i)$ and $z_m(\rho_i)$ are, respectively, the z coordinates of the extrapolations for $\rho_i \in \rho_{common}$ of the cubic smoothing splines approximating *profile_f* and *profile_m*;
- $n_f(\rho_i)$ and $n_m(\rho_i)$ are, respectively, the normal of the extrapolations for $\rho_i \in \rho_{common}$ of the cubic smoothing splines approximating *profile_f* and *profile_m*;

An iterative optimization process, using the Levenberg-Marquardt algorithm[28], adjusts the translation along the z-axis of *profile_m* to minimize error E. The vertical displacement (Δz) is calculated as the average absolute difference between the profiles:

$$\Delta z = \frac{1}{N}\sum_{i=1}^{N}\left|z_f(\rho_i) - z_m(\rho_i)\right| \quad (5)$$

2D profile reconstruction

The 3D point cloud is created by rotating a 2D representation of the external bell profile around its axis of symmetry. However, this method does not automatically include non-axially symmetric decorations, so these features must be manually added to the 3D model based on the specifications provided by the archaeologists.

Results

The devised computer-based method was implemented within the MATLAB® environment and tested against the case study of the reconstruction of a medieval bell from the acquired 3D point clouds of 35 fragments of external mould, as mentioned in "Methods". 3D scanning was performed using a calibrated FARO Edge® 9 ft ($\approx 2.7m$) laser scanner.

According to the technical specification of the scanning device, the repeatability of a single point varies from 0.024 to 0.064 mm, and the average point spacing of the point cloud was set to 0.3 mm. Design X® software package is used to create a manifold model by implementing the procedure suggested in ref. 30. First, outliers are removed. Next, a point cloud for each fragment is generated by aligning two acquisitions taken from opposite viewpoints. Registration is considered successful when the mean distance between the two considered point clouds is less than 0.1 mm. Furthermore, to reach a constant point density of 0.3 mm, a uniform point sampling is carried out after the point clouds are registered. The random noise inevitably derived from the acquisition is removed by using Gaussian smoothing operators so that it does not influence the measurement process. In particular, smoothing ensures that the mean displacement of the points does not exceed a value set to 0.05 mm. Finally, model tessellation and the resolution of non-manifold issues are manually carried out. The automatic analysis method requires the input of the parameters listed in Table 1. These values, set through a preliminary experiment on five random fragments recognized as belonging to the same cluster, ensured the best compromise between smoothness results and computational time.

Of 35 fragments collected by archaeologists, the axes could be calculated for 16 of them. The other fragments 19 were excluded from the dimensional analysis, as their shapes were too poorly defined to be processed by the proposed algorithm for feature segmentation and recognition. For instance, (Fig. 4) illustrates the results of the axis calculation for fragment FR05. The information on the internal wall was inadequate for properly evaluating the axis, whether for preliminary or refinement methods.

Figure 5 shows the results for fragments *FR*#01 (Fig. 5a) of:

- The generation of a digital twin (Fig. 5b) through 3D scanning and the construction of a discrete manifold model *tol*.
- Internal wall segmentation (Fig. 5c) based on identifying the largest area of the fragment's surface with the *sharpness indicator* (SHI)[26] values lower than a specified threshold *tol*;

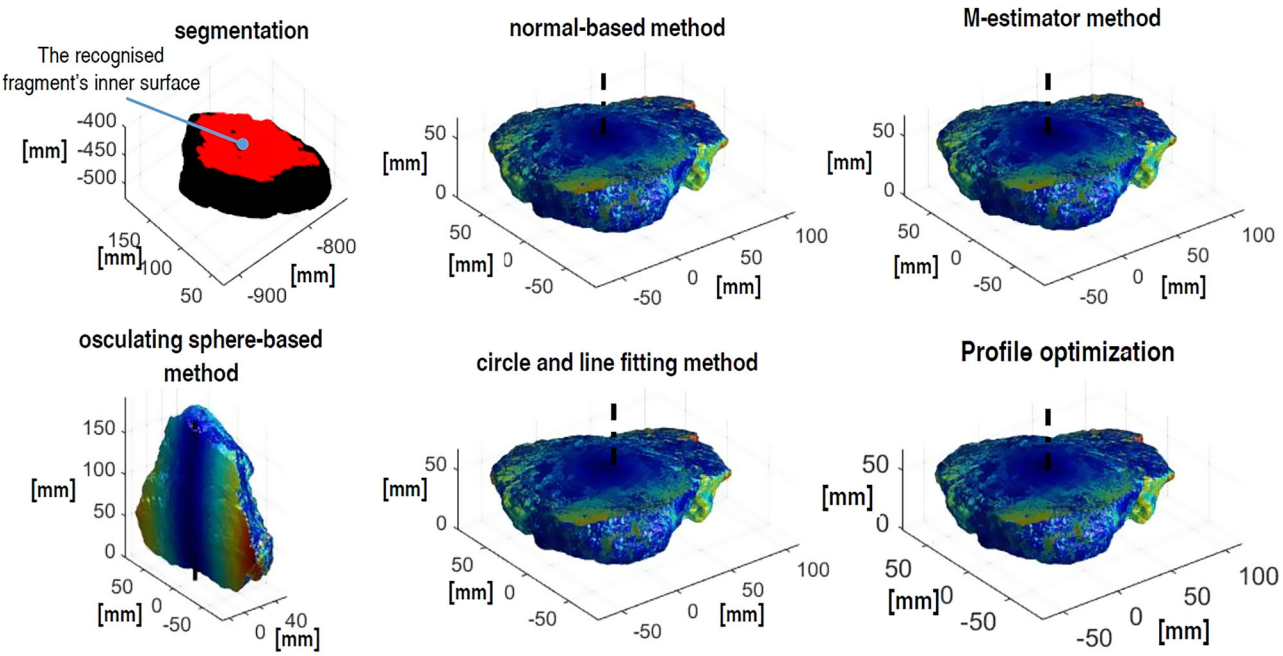


Fig. 4 | Results from the axis estimation for a poorly defined fragment (*FR*#5).

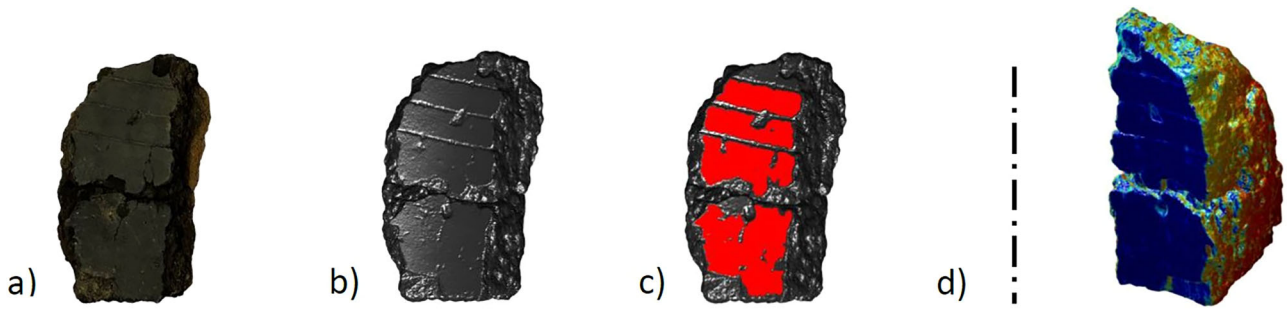


Fig. 5 | Key steps of the proposed methodology allowing axis evaluation of Fragmented Cultural Heritage Assets. a Original fragment *FR*#01; **b** digitalisation; **b** Casting mantle internal wall identification; **c** axis detection; **d** final 3D model of the fragment.

- Axis evaluation (Fig. 5d) resulting from the iterative method that minimizes the

profile area on the internal wall points, starting from an appropriately chosen initial solution *tol*.

The procedure was repeated for the fragments analysed, positioning the z-axis of the x-y-z reference system in alignment with their respective symmetry axes. Out of the 16 fragments analysed, the M-estimator was the first method attempted and had the smallest profile area before refinement. In every case, the refinement process reduced the profile area even further. Therefore, based on these findings, the corresponding axis was considered the fragment axis.

The proposed methodology divided the fragments into five clusters based on their diameter ranges (see Fig. 6a). Figure 6b and 6c illustrate the results of the coarse (Fig. 6b) and fine adjustments (Fig. 6c), achieved by minimizing the objective functions detailed in Eq. 2.

Although all other clusters contain common areas in axial symmetrical zones, fragments *FR*#13 and *FR*#16 share a distinctive characteristic of rounded raised decorations (Fig. 6d). This finding emerges from an analysis of the diameters of these decorations on two different surfaces, revealing three rope decorations.

This conclusion, which differs from previous observations by archaeologists, is substantiated by the fact that the different rope decorations exhibit three distinct characteristic sizes. Figure 6e shows the results of the representative external profile of the bell for each cluster. Figure 6f graphically reports the final positioning of these profiles minimizing the function in equation 4. The profile obtained for K_I was approximated using a cubic spline; the resulting curve was extrapolated downward until the point with vertical tangency was reached.

The relative positions of $K_{IV_{FR\#13}}$ relative to K_{III}, and $K_{IV_{FR\#16}}$ in relation to $K_{IV_{FR\#13}}$ have been updated to consider the thickness of the rope decorations.

As mentioned before, it is not trivial to accurately capture the geometry of the bell's axially symmetric decorations, mainly due to their dimensions (around one to two millimetres), their state of preservation, and the optical accessibility to such features. In the lower section of the reconstructed profile (approximately from z 50 to 150 mm), the shape was inferred based on stylistic analogies with bells from the same period and region. Archaeological drawings and documentation were utilised to support this reconstruction.

The results of adding four circularly contoured embossed ornaments to the bell profile are shown in Fig. 6g. The diameter of the bell base, measured on the final 3D model, is equal to 427.4 mm, which is very close to the estimated value of 430 mm reported by the archaeologists. Figure 6h shows the final model of the bell, which includes three additional decorations of the rope. These non-axially symmetric decorations have been manually added to the 3D model using Computer-Aided Design software. Their shapes and dimensions were

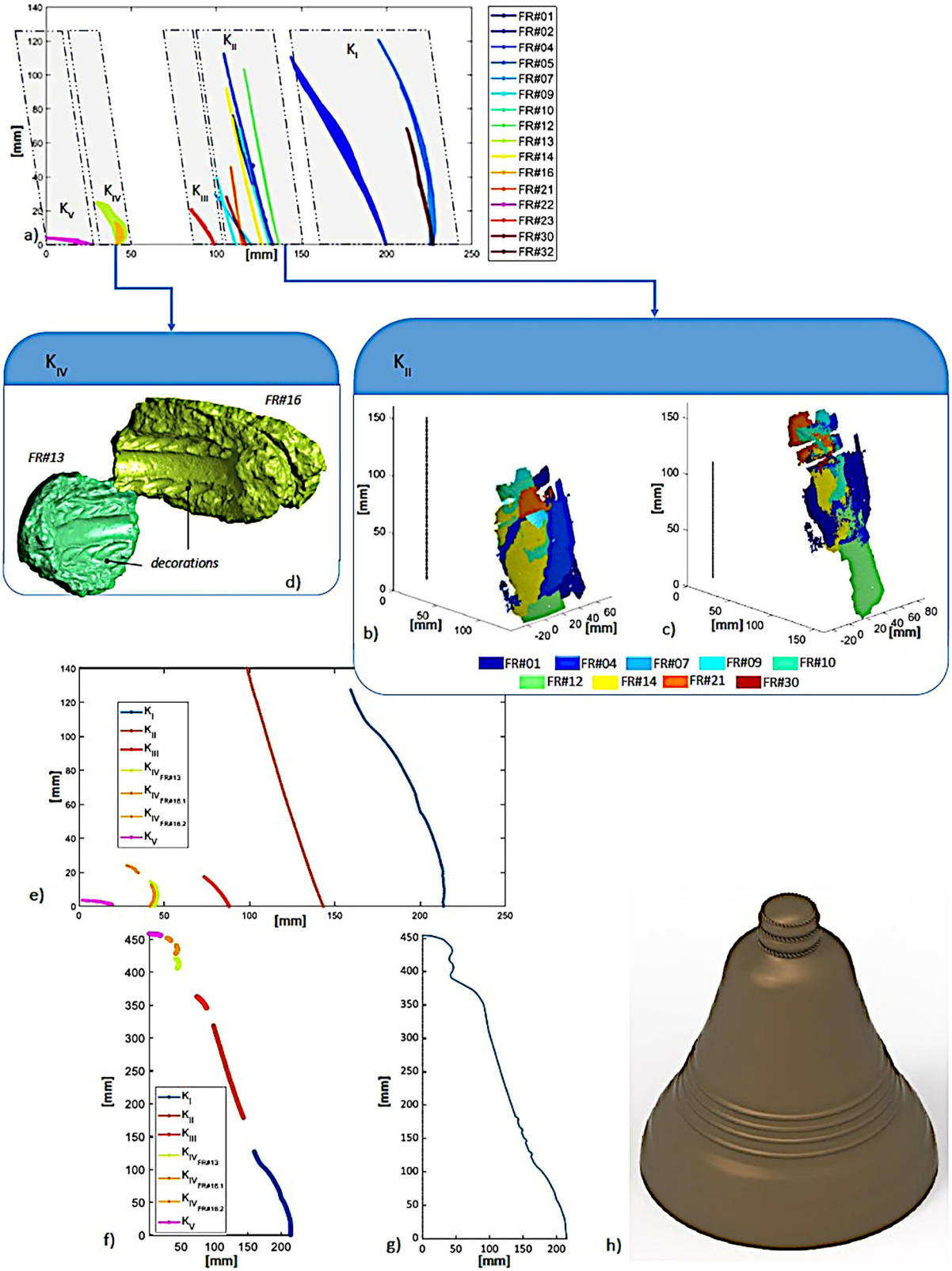


Fig. 6 | Key steps of the proposed methodology used to retrieve the bell geometry from its fragments. a identification of the fragments clusters; **b** coarse registration of the fragments' internal walls of the cluster K_{II}; **c** fine registration of the internal walls of the cluster K_{II}; **d** The registration of fragments *FR*#13 and *FR*#16 based on rounded raised decorations; **e** bell's representative external profile for each cluster; **f** the results of positioning algorithm applied to the representative external profile; **g** external profile of the bell enriched with the axially-symmetric decorations; **h** final 3D surface of the bell with non-axially symmetric decorations.

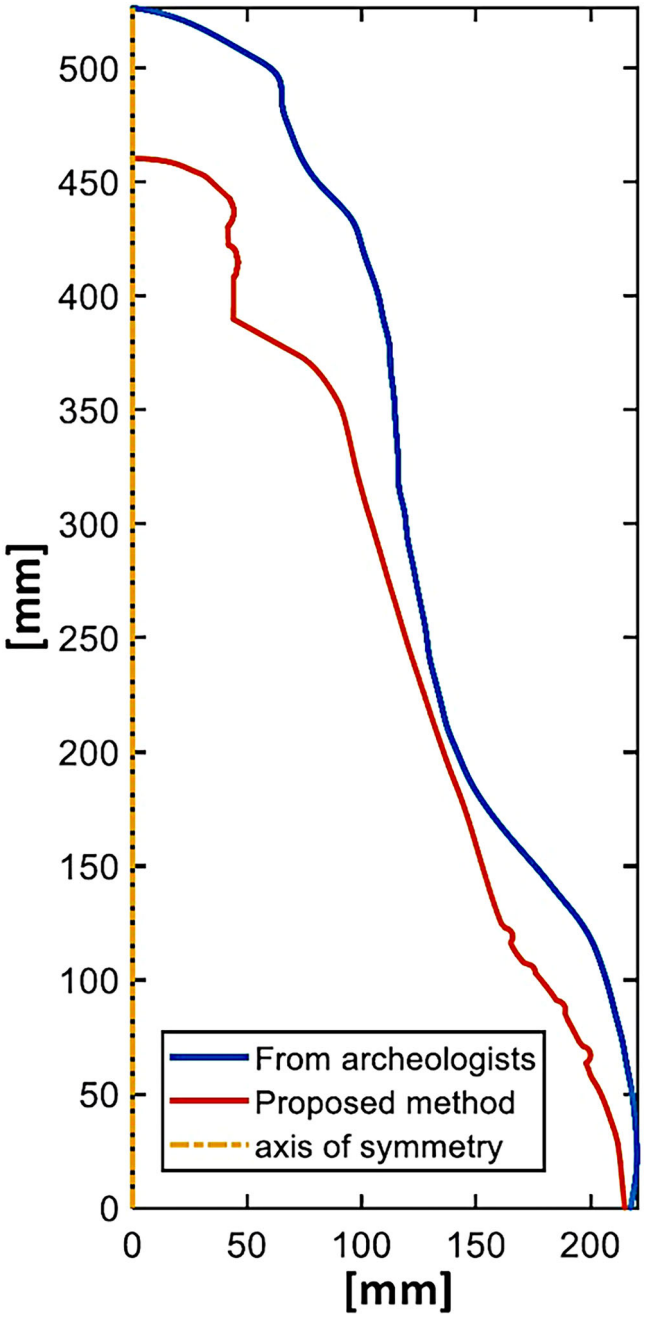


Fig. 7 | The comparison between the axially symmetric profiles obtained by the proposed method and the manual method from archaeologists.

determined by archaeologists who analysed the traces on fragments FR13 and FR16, drawing stylistic comparisons with bells from the same period and region.

The same fragments considered in this paper were analysed by archaeologists using traditional manual methods. The archaeologists selected the 10 most significant fragments (*FR*#1, *FR*#2, *FR*#3, *FR*#4, *FR*#5, *FR*#8, *FR*#13, *FR*#16, *FR*#24, *FR*#25). For each of these fragments, they estimated the spatial orientation and measured the diameters perpendicularly to the estimated axis in increments of 10 cm. The final profile of the bell was created by positioning these diameters perpendicularly to the z-axis, constraining the overall height based on measurements taken during the archaeological excavation of the furnace. Figure 7 compares the two obtained axially symmetric profiles, highlighting the evident differences in shape and dimensions.

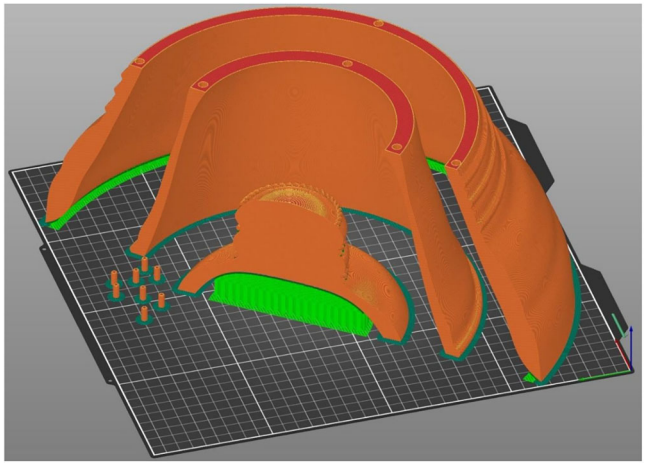


Fig. 8 | The arrangement of the three parts making up the model on the print bed and the use of support material.

Discussion

The significant differences between the profiles obtained using the proposed automatic method and the traditional manual method require a second experiment to verify the reliability of the results obtained with the computer-based method. In particular, the limitation in verifying the reliability of the previously presented results is due to the lack of a 3D model of the bell from which the fragments of the external mould were analysed. The methodology described here includes methods for feature segmentation, recognition, and 2D profile reconstruction. Each of these methods has been evaluated individually in previous studies focused on analysing pottery shards[27,31,32]. Additionally, a fine registration approach was used to realign and register point clouds obtained from scanning upper limb anatomy with a depth-camera-based scanner[29]. Since the level of information available for bell reconstruction was considered comparable to that found in the cited studies, it was determined that retesting these methods was unnecessary. Instead, the focus was placed on assessing the reliability of the overall methodology. To address this issue, in the new experiment, a 3D model of the bell from the method proposed in "Results" was produced through additive manufacturing and subsequently acquired using a scanner. The external surface of the reconstructed bell was algorithmically divided into patches, on which the proposed method was applied. The choice to use a 'physical reference model' for testing and validating the proposed methodology is motivated by the need for more reliable results. By employing real data, which includes inherent errors from its collection, we can attain greater accuracy than we would with synthetic meshes that incorporate artificial Gaussian errors. The 3D model is constructed using the Prusa XL printer, which has a build volume of 360 mm × 360 mm x 360 mm, allowing the execution of large-scale projects. Since the bell model had a diameter of 430 mm and a height of 530 mm, careful planning was required for effective printing and assembly. The CAD model was divided into three parts along three horizontal planes to optimize the print and reduce the use of support materials. This strategic division allowed efficient printing of the upper sections while minimizing the waste of support material and preserving surface quality.[33,34] The alignment holes for dowels were designed in each division plane to maintain precise alignment during assembly[35].

Although two dowels per plane would suffice, a third was added to help mitigate any potential deformation in the components, ensuring better fit and assembly accuracy. The 3D models were placed on the print bed with the largest diameter aligned roughly parallel to the diagonal of the print bed, thus maximizing the usage of print space and reducing print time (all parts could be printed with a single job), according to ref. 36. This arrangement allowed for a seamless print of each section without further subdivisions. The arrangement of the three parts that make up the model on the print bed and the use of support material are shown in Fig. 8. The CAD model has

Table 2 | Key printing setting

Settings	
Material	PLA
Filament Diameter	1.75 mm
Extrusion Temperature	220 °C
Extrusion nozzle diameter	0.4 mm
Layer Thickness	0.25 mm
Perimeters for Vertical Walls	Minimum of 2
Solid Layers for Horizontal Walls	Minimum of 4
Infill Density	15%, using a grid structure
Overhang Support Threshold	45°
Printing Speed	Variable, between 50 and 140 mm/s

meshed with a 0.3 mm mesh size to avoid "faceting" errors and ensure a smooth, accurate print[34]. Table 2 summarizes the key print settings; this approach and these parameters facilitated a high-quality, efficient print while ensuring structural integrity and ease of assembly for the bell model.

The printed model (Fig. 9a) was acquired using the same scanner as in "Results" keeping the average point spacing of the point cloud set to 0.3 mm. Figure 9b illustrates the distance map between the synthetic and acquired bells, revealing that 91.24% of the distances fall below the density points. Figure 11 displays the 16 original internal wall patches registered on the 3D model obtained from the scan. The angular position was randomly defined since the model was derived from a symmetrical profile. The patches for analysis were extracted from the acquired surface as the points closest to the fragment patches. The 16 patches were then analysed using the algorithm discussed in this paper.

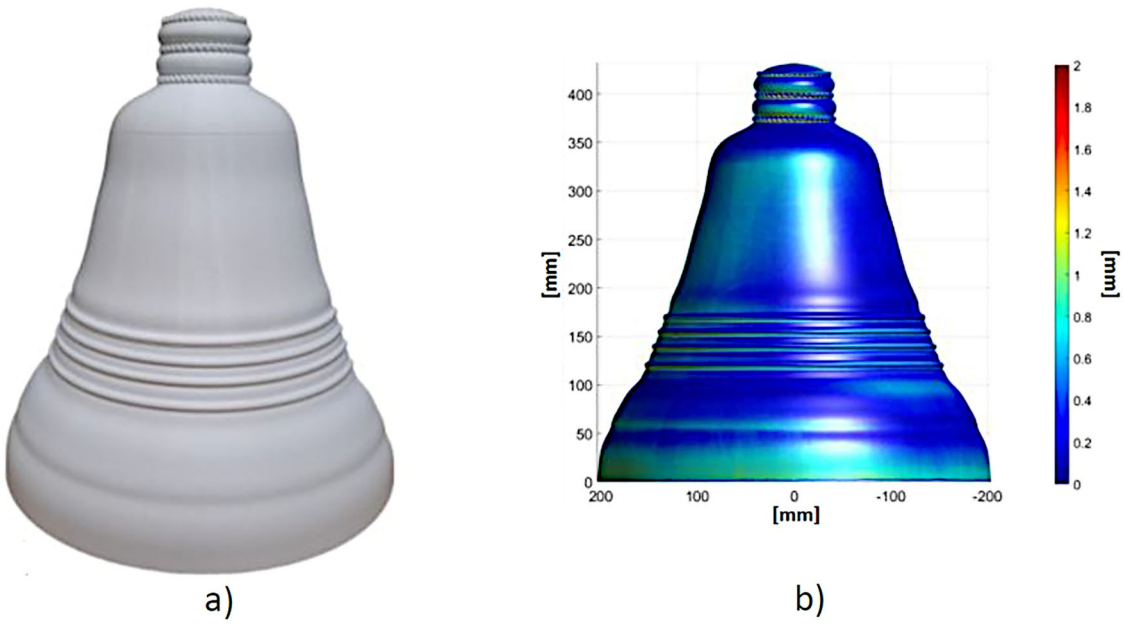


Fig. 9 | 3D bell printed model. a Digital model; **b** corresponding map of the distance between the synthetic and scanned 3D model.

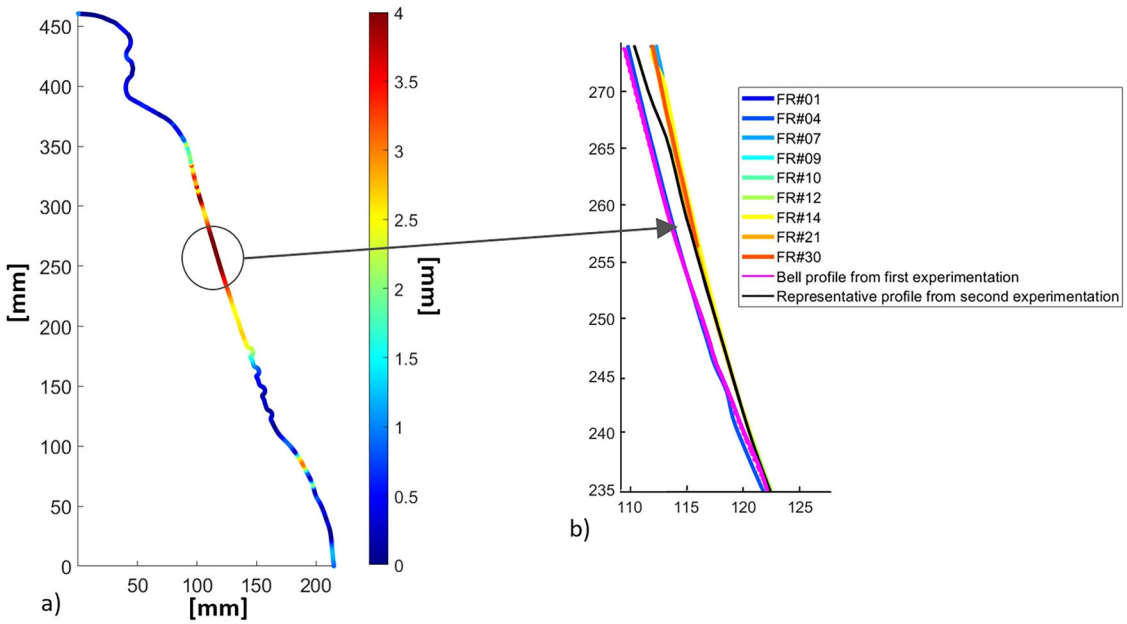


Fig. 10 | Comparison between the profiles coming from the first and second experimentations. a Distance map between the profiles; **b** zoom in on the area at the maximum distance.

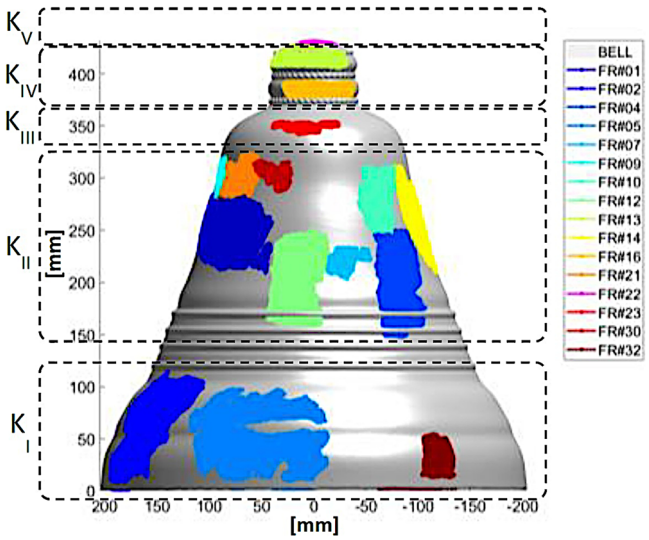


Fig. 11 | The 16 fragments' internal walls patches registered on the 3D bell scanned model.

Figure 10a) illustrates the negligible differences between the two profiles of the two experiments, with a maximum distance of less than 5 millimetres. Figure 10a) indicates that the maximum distance results from registration errors in the area with the greatest overlap of fragments. While the method cannot guarantee convergence to a global minimum, it consistently delivers satisfactory results. Based on deterministic algorithms, the proposed method produces similar results starting from a comparable input. However, evaluating the reliability of the resulting shape is difficult because of the noisy and incomplete information available. The zones K_I, K_{II}, and K_V are well approximated by the fragments and are associated with areas with a nearly constant curvature profile. This consistent profile allows for a reliable connection with the adjacent shapes. In contrast, the areas K_{III} and K_{IV} are only roughly represented (as shown in Fig. 11). As a result, the current representation is less reliable in the K_{III} and K_{IV} areas where the available information is limited.

Accordingly, this study introduced a new computer-based method devoted to reconstructing fragmented axially symmetric cultural heritage assets, specifically applied to a medieval bell. Due to the challenge of reassembling fragments of its external mould on their fracture surfaces, traditional manual approaches used by archaeologists rely on estimations regarding the spatial orientation of significant fragments. These approaches measure diameters perpendicular to the estimated axis at set increments.

The final profile of the bell is constructed by positioning these diameters perpendicular to the z-axis, with the overall height constrained based on measurements taken during the archaeological excavation of the furnace. The results of these methods, which are neither repeatable nor reproducible, depend heavily on the preparation, experience, and expectations of the operators rather than on a thorough analysis of the fragments themselves. In contrast, the proposed method employs geometric differential analysis and 3D scanning to address these limitations and accurately reconstruct the shape of the bell from its casting mould mantle fragments.

This approach aims to recreate the bell's three-dimensional form using its two-dimensional profile, utilizing a custom-developed geometric-differential analysis of the discrete models obtained from a 3D scanner. The process was applied to 35 fragments of the external mould excavated from a medieval bell furnace in inland Abruzzo. Specific experiments were conducted to assess the precision, potential, and limitations of the procedure implemented. The method successfully produces a shape consistent with bells from the same region and time period. Significant differences in accuracy and detail were observed compared to conventional manual reconstructions performed by archaeologists, highlighting the effectiveness of the digital method. Furthermore, the reliability of the method in reconstructing axially symmetric objects was validated through additive manufacturing and scanning of a synthetic model. To the best of our knowledge, no published work currently presents a computer-based method for reconstructing globally axially symmetric 3D models from fragments without relying on the assembly of fractured surfaces. This is particularly significant when reconstructing the original shapes of archaeological finds that have been lost and when remaining fragments cannot be joined along their fractured surfaces. Given these promising results, future efforts will focus on extending the analysis to different furnaces and validating the method in cases where a physical model is also available. Implementing the proposed method for its application to other archaeological artifacts, such as pottery, will also be one of the main focuses of future work on this topic. As part of future validation efforts, the method will be tested in scenarios where physical reference models are available, allowing for a more comprehensive assessment of its accuracy.

Data availability

No datasets were generated or analysed during the current study.

Received: 28 January 2025; Accepted: 21 September 2025;
Published online: 09 October 2025

References

1. Munteanu, S. I., Ciobanu, I. & Ene, V. The heaviest cast bells existing in the world-art of castings. *Metal. Int.* **16**, 56 (2011).
2. Debut, V., Carvalho, M., Figueiredo, E., Antunes, J. & Silva, R. The sound of bronze: Virtual resurrection of a broken medieval bell. *J. Cult. Herit.* **19**, 544–554 (2016).
3. Zhang, D., Shan, Y., Chen, X. & Wang, Z. Soundscape in religious historical buildings: a review. *Herit. Sci.* **12**, 45 (2024).
4. Roda, A., De Poli, G., Canazza, S., Sun, Z. & Whiting, E. 3D virtual reconstruction and sound simulation of old musical instruments. *Archeol. Calc.* **32**, 359–374 (2021).
5. Koumartzis, N., Tzetzis, D., Kyratsis, P. & Kotsakis, R. G. A new music instrument from ancient times: modern reconstruction of the Greek lyre of Hermes using 3D laser scanning, advanced computer aided design and audio analysis. *J. N. Music Res.* **44**, 324–346 (2015).
6. Rossing, T. D. & Perrin, R. Vibrations of bells. *Appl. Acoust.* **20**, 41–70 (1987).
7. Cekus, D. & Nadolski, M. Assessment of the change in the tin concentration in bronzes to the basic components of the sound of bells. *Arch. Metal. Mater.*, 531–535 (2021).
8. Cekus, D., Kwiatoń, P., Nadolski, M. & Sokół, K. Effect of material-technological properties on the reconstruction of utility parameters of bells. *Eng. Sci. Technol., Int. J.* **24**, 1042–1048 (2021).
9. Lehr. A. The geometrical limits of the carillon bell. Acta Acustica United with Acustica **86**, 543–549.
10. Figueiredo, E., Valerio, P., Fátima Araújo, M., Rui Silva, J. C. & Monge Soares, A. M. Inclusions and metal composition of ancient copper-based artefacts: a diachronic view by micro-EDXRF and SEM-EDS. *X-Ray Spectrom.* **40**, 325–332 (2011).
11. Fletcher, N. H., McGee, W. T. & Tarnopolsky, A. Z. Bell clapper impact dynamics and the voicing of a carillon. *J. Acoust. Soc. Am.* **111**, 1437–1444 (2002).
12. Woodhouse, J. et al. The dynamics of a ringing church bell. *Adv. Acoust. Vib.* **2012**, 681787 (2012).
13. Brzeski, P., Kapitaniak, T. & Perlikowski, P. Experimental verification of a hybrid dynamical model of the church bell. *Int. J. Impact Eng.* **80**, 177–184 (2015).
14. Brzeski, P., Chong, A. S. E., Wiercigroch, M. & Perlikowski, P. Impact adding bifurcation in an autonomous hybrid dynamical model of church bell. *Mech. Syst. Signal Process.* **104**, 716–724 (2018).
15. Siebert, A., Blankenhorn, G. & Schweizerhof, K. Investigating the vibration behavior and sound of church bells considering ornaments

and reliefs using LS-DYNA. 9th International LS-DYNA Users Conference: conference proceedings. **8** 2006.
16. Carvalho, M., Debut, V. & Antunes, J. Physical modelling techniques for the dynamical characterization and sound synthesis of historical bells. *Herit. Sci.* **9**, 1–17 (2021).
17. Cekus, D., Kwiatoń, P., Nadolski, M. & Sokół, K. Quality assessment of a manufactured bell using a 3D scanning process. *Sensors* **20**, 7057 (2020).
18. Redi, F., Forgione, A., Savini, F., Amoretti, V. & Di Pietro, T. S. Lucia di Rocca di Cambio (AQ), campagna di scavo 2010 [S. Lucia di Rocca di Cambio (AQ), excavation campaign 2010]. *S. Lucia Rocca Cambio (AQ), Camp. Scavo* **2010**, 255–276 (2011).
19. Colin R. & Paul B. Archaeology: Theories, Methods, and Practice. 7th. London: Thames & Hudson, 2016.
20. Di Angelo, L., Di Stefano, P. & Guardiani, E. A review of computer-based methods for classification and reconstruction of 3D high-density scanned archaeological pottery. *J. Cult. Herit.* **56**, 10–24 (2022).
21. Forgione, A. Una fornace da campana dalle indagini del complesso monastico di S. Lucia di Rocca di Cambio (AQ) [A bell furnace from the investigations of the monastic complex of S. Lucia di Rocca di Cambio (AQ)]. Archeologia medievale: cultura materiale, insediamenti, territorio: XXXVIII, 277-285 (2011).
22. Di Angelo, L., Di Stefano, P., Forgione, A., Guardiani, E. & Morabito, A. E. A New Computer-Based Method for Digital Reconstruction of Archeological Bells from the Fragments of Their Casting Mantle. International Conference of the Italian Association of Design Methods and Tools for Industrial Engineering. Springer, 235-243 (2024).
23. Chen, L., Feng, C., Ma, Y., Zhao, Y. & Wang, C. A review of rigid point cloud registration based on deep learning. *Front. Neurorobot.* **17**, 1281332 (2024).
24. Ning, X., Li, F., Tian, G. & Wang, Y. An efficient outlier removal method for scattered point cloud data. *PloS one* **13**, e0201280 (2018).
25. Dinesh, C., Cheung, G. & Bajić, I. V. Point cloud denoising via feature graph Laplacian regularization. *IEEE Trans. Image Process.* **29**, 4143–4158 (2020).
26. Di Angelo, L. & Di Stefano, P. C1 continuities detection in triangular meshes. *Comput.-Aided Des.* **42**, 828–839 (2010).
27. Di Angelo, L., Schmitt, A., Rummel, M. & Di Stefano, P. Automatic analysis of pottery sherds based on structure from motion scanning: The case of the Phoenician carinated-shoulder amphorae from Tell el-Burak (Lebanon). *J. Cult. Herit.* **67**, 336–351 (2024).
28. S. Sapna, A. Tamilarasi, and M. Pravin Kumar. Backpropagation learning algorithm based on the Levenberg-Marquardt Algorithm. In: *Comp Sci Inform Technol (CS and IT)* 2 (2012), 393–398.
29. Di Angelo, L. et al. Automatic Multiview Alignment of RGB-D Range Maps of Upper Limb Anatomy. *: Sens.* **23**, 7841 (2023).
30. M. Berger, *et al*. "A survey of surface reconstruction from point clouds". In: *Computer graphics forum*. Vol. 36. Wiley Online Library. 2017, 301–329.
31. L. Di Angelo, P. Di Stefano, E. Guardiani, and C. Pane. Automatic shape feature recognition for ceramic finds. In: *J. Comput. Cult. Herit. (JOCCH)* 13(2020), 1–21.
32. L. Di Angelo, P. Di Stefano, and A. Eva Morabito Comparison of methods for axis detection of high-density acquired axially-symmetric surfaces". In: *Int. J. Interact. Design Manuf. (IJIDeM)* 8 (2014), 199–208.
33. Zhang, Y., Bernard, A., Harik, R. & Karunakaran, K. P. Build orientation optimization for multi-part production in additive manufacturing. *J. Intell. Manuf.* **28**, 1393–1407 (2017).
34. Mary K. et al. Design for Additive Manufacturing: Trends, opportunities, considerations, and constraints. In: *CIRP Annals* 65.2 (2016), 737–760.
35. Buonamici, F. et al. Optimizing fabrication outcome in low-cost FDM machines. Part 1-metrics. *Manuf. Technol.* **18.3**, 372–378 (2018).
36. I. E. Moyer, S. Bourgault, D. Frost, and J. Jacobs. Don't Mesh Around: Streamlining Manual-Digital Fabrication Workflows with Domain-Specific 3D Scanning. In: *Proceedings of the 37th Annual ACM Symposium on User Interface Software and Technology*. 2024, 1–16.

Acknowledgements

We sincerely thank Prof. Alfonso Forgione, Associate Professor of Christian and Medieval Archaeology at the University of L'Aquila, for his invaluable contributions to this study. His expertise and insights were crucial in completing this research.

Author contributions

L.D.A. conceptualized and established the methodology, implemented the algorithms, conducted the experiments, conducted the formal analysis of the results, contributed to drafting the original manuscript, and subsequently reviewed and edited the paper. PDS supervised the project and participated in the review and editing of the paper. L.G. and R.F. designed the manufacturing process for the 3D model of the bell, drafted the original manuscript, and subsequently reviewed and edited the paper. E.G. contributed to developing the methodology, implemented the algorithms, conducted the experiments, performed a formal analysis of the results, and drafted the original manuscript. All authors read and approved the final manuscript.

Competing interests

The authors declare no competing interests.

Additional information

Correspondence and requests for materials should be addressed to Rocco Furferi.

Reprints and permissions information is available at http://www.nature.com/reprints

Publisher's note Springer Nature remains neutral with regard to jurisdictional claims in published maps and institutional affiliations.

Open Access This article is licensed under a Creative Commons Attribution-NonCommercial-NoDerivatives 4.0 International License, which permits any non-commercial use, sharing, distribution and reproduction in any medium or format, as long as you give appropriate credit to the original author(s) and the source, provide a link to the Creative Commons licence, and indicate if you modified the licensed material. You do not have permission under this licence to share adapted material derived from this article or parts of it. The images or other third party material in this article are included in the article's Creative Commons licence, unless indicated otherwise in a credit line to the material. If material is not included in the article's Creative Commons licence and your intended use is not permitted by statutory regulation or exceeds the permitted use, you will need to obtain permission directly from the copyright holder. To view a copy of this licence, visit http://creativecommons.org/licenses/by-nc-nd/4.0/.

© The Author(s) 2025